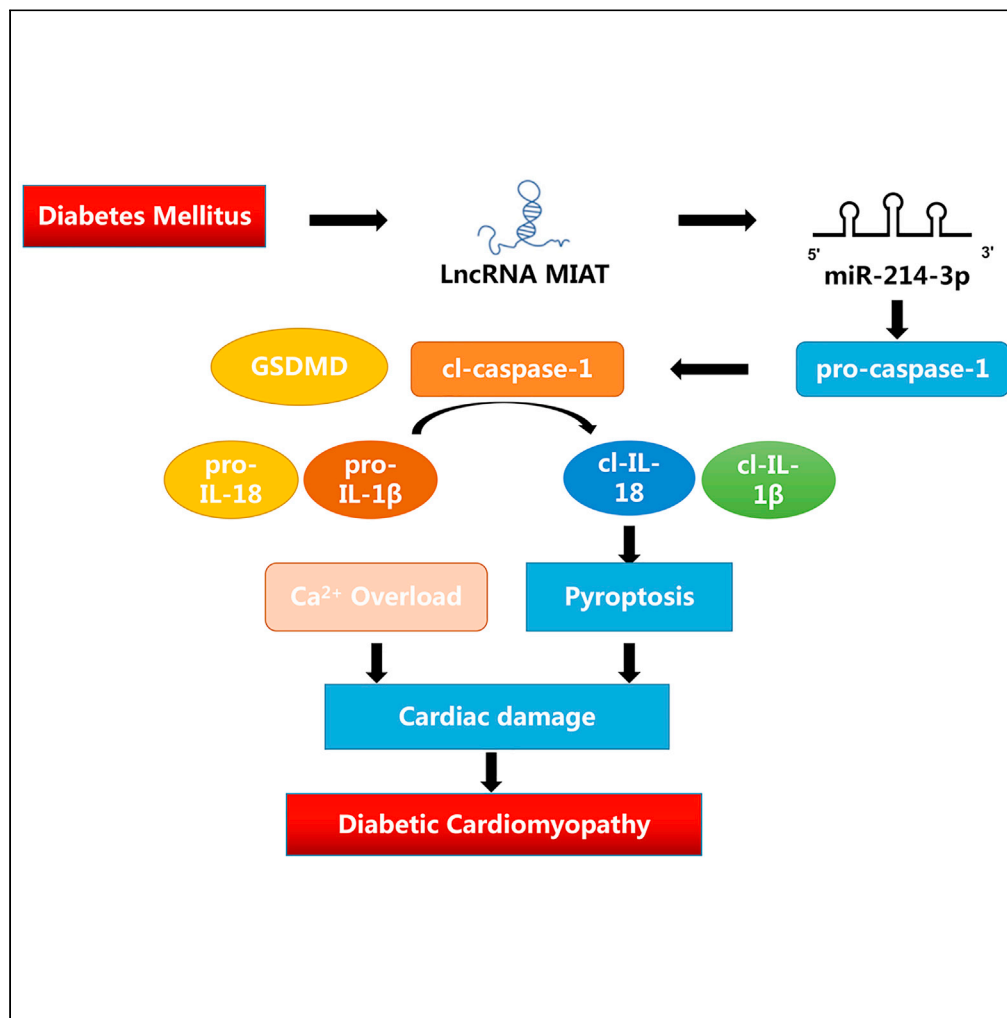# iScience

Article

Long non-coding RNA MIAT is involved in the regulation of pyroptosis in diabetic cardiomyopathy via targeting miR-214-3p

Wenjing Xiao, Dezhi Zheng, Xin Chen, ..., Xudong Wen, Yonghe Hu, Jun Hou

wenxd131@163.com (X.W.)
huyonghezyy@163.com (Y.H.)
jun_hou@yeah.net (J.H.)

Highlights

MIAT and caspase-1 were overexpressed in serum and cardiomyocytes of diabetic patients

High glucose caused inflammatory damage and calcium overloaded in cardiomyocytes

MIAT regulated pyroptosis in cardiomyocytes via MIAT-miR-214-3p-CASP1 axis

Article

Long non-coding RNA MIAT is involved in the regulation of pyroptosis in diabetic cardiomyopathy via targeting miR-214-3p

Wenjing Xiao,[1,2,6,7] Dezhi Zheng,[3,6] Xin Chen,[4,6] Botao Yu,[2] Kaiwen Deng,[2] Jie Ma,[2] Xudong Wen,[5,*] Yonghe Hu,[1,2,*] and Jun Hou[1,2,*]

SUMMARY

Diabetic cardiomyopathy (DCM) is one of the most common complications of diabetes without effective treatment options. Its pathogenesis is complex and remains unclear. Long non-coding RNA (lncRNA) MIAT allele has been reported to be enriched in DCM patients and activate a pyroptosis program in hypoxia-induced H9c2 cells. Thus, whether MIAT played a role in DCM pyroptosis remains to be clarified. In the study, the expression of MIAT was found elevated in the serum of diabetic patients, as well as in high-glucose induced cardiomyocytes and diabetic mice. Further, the expression levels of CASP1 and pyroptosis correlation factors (IL-1 and IL-18) were downregulated after silencing MIAT. Through modeling and validation experiments, we then confirmed that the MIAT-miR-214-3p-CASP1 axis serves as an essential point in pyroptosis of DCM mice. These results suggested that silencing MIAT would be a potential treatment strategy for DCM.

INTRODUCTION

Diabetes mellitus (DM) is a metabolic disorder syndrome caused by an absolute or relative lack of insulin secretion and characterized by hyperglycemia and hyperlipidemia (Mohanty and Das, 2017). Diabetic cardiomyopathy (DCM) is one of the most serious complications of DM and is a major cause of heart failure, arrhythmia, and even sudden death (Bulani and Sharma, 2017). However, the detailed molecular mechanism of DCM is still unclear, resulting in limited options for disease treatment. Therefore, our in-depth study of its pathogenesis might provide a theoretical basis for the development of an effective treatment option for DCM.

Long non-coding RNAs (lncRNAs) are a type of RNA, defined as being transcripts with lengths exceeding 200 nucleotides that are not translated into protein (Niu et al., 2017). LncRNAs feature as poor conservation between species and high specificity for cell expression. It was well-established that lncRNAs were involved in almost all physiological processes, regulating cell proliferation, differentiation, and metabolism (Lee and Kikyo, 2012; Novikova et al., 2012). They were also involved in the onset of various diseases that include cancer, diabetes, immune diseases, and Alzheimer's disease (Knauss and Sun, 2013; Peng et al., 2010). LncRNA myocardial infarction-associated transcription (MIAT) allele is an lncRNA enriched in the diabetic cardiomyocytes, acting as a competing endogenous RNA (ceRNA) that forms a feedback loop with vascular endothelial growth factor and miR-150-5p to regulate endothelial cell function. In a previous large-scale, case-control study conducted in Japan, MIAT allele was reported to be associated with myocardial infarction. Other studies reported that lncRNA MIAT was associated with a diversity of pathogenesis including gastric cancer proliferation and metastasis (Sha et al., 2018), microvascular dysfunction (Yan et al., 2015), myocardial ischemia-reperfusion injury (Liu et al., 2019), and diabetes (Zhou et al., 2017). MicroRNAs (miR-NAs) were well-established to regulate many physiological processes via sponging mRNAs (Qi et al., 2020). Previous study revealed that miR-214-3p has binding sites with caspase-1 and could regulate pyroptosis in DCM. Recently, it was found that miRNAs could also interact with lncRNAs. It was reported that MIAT targets miR-214-3p in diabetic mice, regulating the secretion of IL-17 (Qi et al., 2020). As a result, it is believed that the interaction between MIAT and miR-214-3p is likely to be involved in the pathogenesis of DCM.

Pyroptosis is a lytic form of cell death, which is induced by inflammatory caspases upon activation of the canonical or noncanonical inflammasome pathways (Ruhl et al., 2018). Emerging studies showed that

[1]School of Materials Science and Engineering, Southwest Jiaotong University, Chengdu 611756, China

[2]Department of Pharmacy, The General Hospital of Western Theater Command of PLA, No 270 Rongdu Road, Jinniu District, Chengdu 610083, China

[3]Department of Cardiovascular Surgery, The 960th Hospital of the PLA Joint Logistic Support Force, Jinan 250031, China

[4]Affiliated Hospital of Southwest Jiaotong University & The Third People's Hospital of Chengdu, Chengdu 610015, China

[5]Department of Gastroenterology and Hepatology, Chengdu First People's Hospital, Chengdu 610016, China

[6]These authors contributed equally

[7]Lead contact

*Correspondence:
wenxd131@163.com (X.W.),
huyonghezyy@163.com (Y.H.),
jun_hou@yeah.net (J.H.)

https://doi.org/10.1016/j.isci.2021.103518

pyroptosis was also involved in the pathogenesis of DCM (Luo et al., 2017; Yang et al., 2018). For example, nucleotide-binding oligomerization domain-like receptor pyrin domain containing 3 (NLRP3) played an important role in regulating cardiomyocyte death and fibroblast activation (Yang et al., 2019b). Moreover, it was reported that pyroptosis was markedly activated in the cardiomyocytes subjected to high-glucose conditions, and miR-214-3p regulated the expression of caspase-1 (Yang et al., 2019a). Considering above-mentioned facts, we hypothesize that MIAT-miR-214-3p-caspase-1 (CASP1) axis is responsible for pyroptosis in high-glucose-induced cardiomyopathy, contributing to the development of DCM.

In this study, our results found that MIAT regulated caspase-1 by targeting miR-214-3p both *in vivo* and *in vitro*. Here, we characterized the expression of MIAT in DCM and studied the mechanism by which MIAT-miR-214-3p-CASP1 axis contributed to the pyroptosis in DCM.
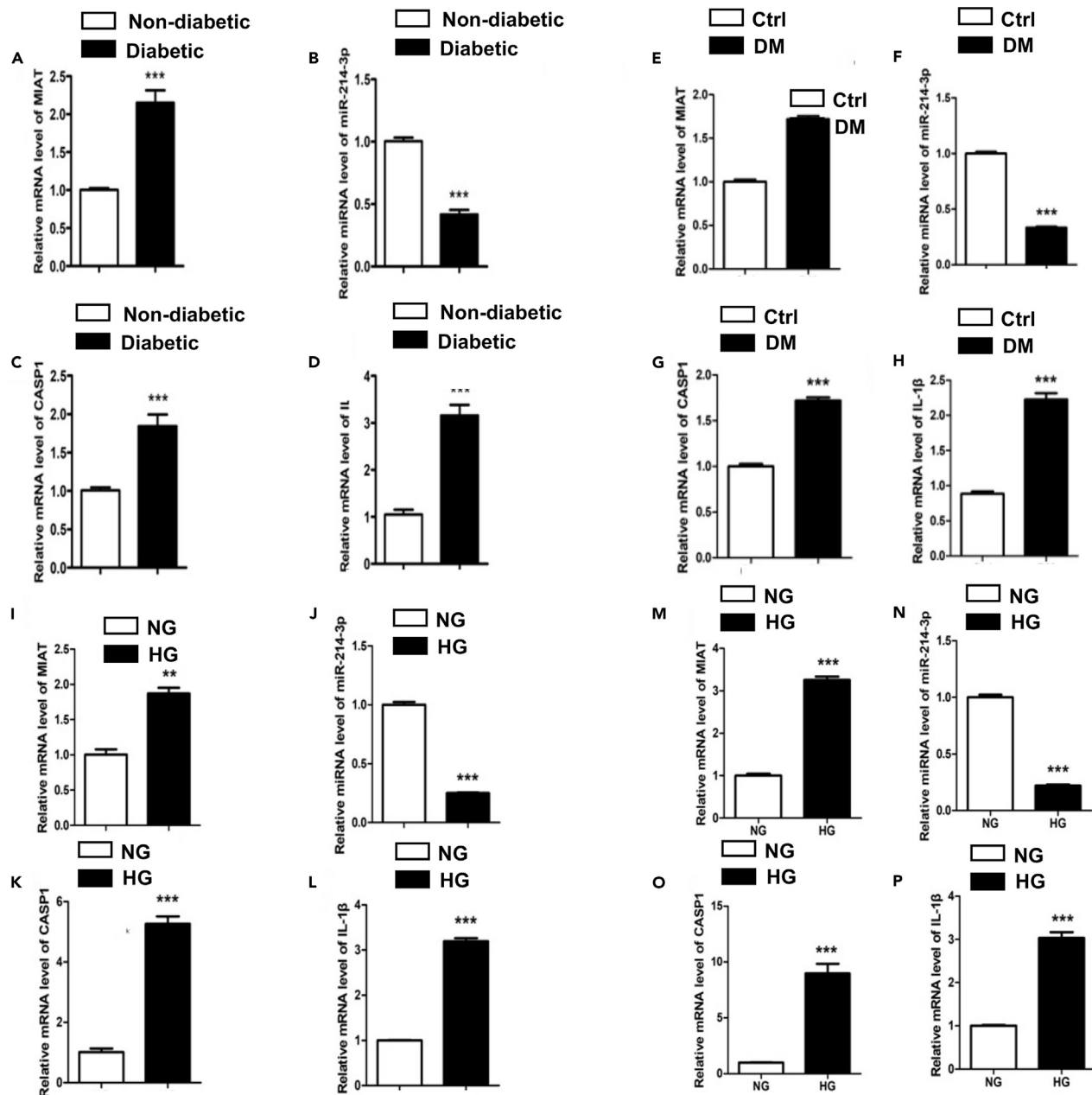
RESULTS

LncRNA MIAT and caspase-1 were overexpressed in the serum of diabetic patients and high glucose-induced cardiomyocytes

It is well-documented that inflammation played a crucial role in the complex pathogenesis of DCM (Bulani and Sharma, 2017). Recently, several lncRNAs including MIAT and KCNQ1OT1 have been reported to be associated with DCM via inflammation mechanism. To clarify the potential roles of lncRNA in the development of DCM, we first measured mRNA expressions of MIAT, miR-214-3p, a potential target of MIAT, and CASP1 and IL-1β, two markers of pyroptosis in the serum of diabetic patients. Our results found that expression levels of MIAT, CASP1, and IL-1β were upregulated, whereas the expression level of miR-214-3p was downregulated in the serum of diabetic patients (Figures 1A–1D). The detail medical records of subjects have been uploaded as attachments and basic data as following table (Tables 1 and 2). To further confirm whether this phenomenon is repeatable or not, we performed the same experiment using an *in vivo* model. The mouse hearts were collected at the end of the experiment. Heart homogenates were processed for the qPCR analysis. The results demonstrated that expressions of MIAT, CASP1, and IL-1β were upregulated, whereas the expression of miR-214-3p was downregulated in DM mice, as compared with healthy controls (Figures 1E–1H). To determine if this change was caused by glucose metabolism, we set up an *in-vitro* model using mouse primary cardiomyocytes. The cells were treated with either normal glucose (NG, 5.5 mmol/L) or high glucose (HG, 25 mmol/L) as mentioned. mRNA expressions of MIAT, miR-214-3p, CASP1, and IL-1β from both cell supernatants and cell lysates were then measured by qRT-PCR. Consistent with the results in diabetic patients, we showed that expressions of MIAT, CASP1, and IL-1β were upregulated, whereas expression of miR-214-3p was downregulated in HG group in both supernatants and cell lysates, as compared with NG group (Figures 1I–1P). Taken together, these results suggest that MIAT is likely to be associated with IL-1β-mediated inflammation, regulated by glucose metabolism.

High glucose treatment caused inflammatory damage and calcium overload in cardiomyocytes

Pyroptosis is triggered by caspase-1 after its activation by various inflammasomes. Subsequently, it results in lysis of the affected cell. Because a higher expression level of CASP1 was observed in the serum from diabetic patients, we questioned if these results were caused by high-glucose-induced cardiac-damage. We therefore investigated the protein expression levels of pro-IL-1β, IL-1β, pro-CASP1, CASP1, pro-IL-18, IL-18, and GSDMD in primary cardiomyocytes. The results demonstrated that the protein expression levels of CASP1, IL-1β, IL-18, and GSDMD were significantly increased in the HG group, as compared to controls (Figures 2A and 2B). Next, to determine whether pyroptosis subsequently happened in cardiomyocytes, we performed transmission electron microscopy to capture the morphological changes of cardiomyocytes upon HG treatment. The results showed that HG-treated cardiomyocytes exhibit pro-inflammatory damage with a hypertrophic morphology, as well as swollen fibril and mitochondria, indicating a potential mechanism by which HG caused cardiac damage via pyroptosis (Figure 2C). Heart muscle is acutely sensitive to inflammation, contributing to the malfunction of the ion channel. It was reported that IL-1β-mediated regulation of calcium channels on the cell membrane was responsible for calcium influx and subsequent calcium overload. To test this mechanism in our model, we applied human primary cardiomyocytes to determine the mechanism by which cell pyroptosis leads to calcium overload. The cells were treated with HG to induce cell pyroptosis. Our results showed that calcium overload was significantly increased upon HG treatment, as compared to control treatment (Figures 2D and 2E). Taken together, these results suggest that abnormal glucose metabolism may cause cardiac damage via two mechanisms: 1) HG-induced cardiomyocyte pyroptosis and 2) HG-induced intracellular calcium overload.

Figure 1. LncRNA MIAT and caspase-1 were overexpressed in the serum of diabetic patients and high glucose-induced cardiomyocytes

(A–D) The relative gene expression levels of MIAT (A), miR-214-3p (B), CASP1 (C), and IL-1β (D) in the serum of non-diabetic and diabetic patients, n = 12. ***p < 0.001 versus the non-diabetic group.

(E–H) The relative gene expression levels of MIAT (E), miR-214-3p (F), CASP1 (G), and IL-1β (H) in the heart homogenate of non-diabetic and diabetic mice, n = 5. ***p < 0.001 versus the control group.

(I–P) The relative gene expression levels of MIAT (I), miR-214-3p (J), CASP1 (K), and IL-1β (L) in the cell supernatants of primary cardiomyocyte and the relative gene expression levels of MIAT (M), miR-214-3p (N), CASP1 (O), and IL-1β (P) in the cell lysates of primary cardiomyocyte. All experiments were performed at least 3 times. ***p < 0.001 versus the NG group.

Verification of binding between MIAT and miR-214-3p

Next, we studied the mechanism by which HG treatment induced the increase of caspase-1. HG treatment treatment also alters the expression of MIAT and miR-214-3p together with the expression of caspase-1. We hypothesize that the regulation of caspase-1 may be caused by the MIAT-miR-214-3p axis. To test the hypothesis, we

Table 1. Data of subjects in the diabetes group

No.	A prior history of diabetes	Cardiac function	Age	Gender
D1	Type 2 diabetes	Normal	60	Female
D2	Type 2 diabetes	Normal	64	Male
D3	Type 2 diabetes	Normal	65	Male
D4	Type 2 diabetes	Normal	67	Male
D5	Type 2 diabetes	Normal	64	Male
D6	Type 2 diabetes	Normal	61	Female
D7	Type 2 diabetes	chronic cardiac insufficiency NYHA class II	67	Female
D8	Type 2 diabetes	Normal	60	Male
D9	Type 2 diabetes	Normal	63	Female
D10	Type 2 diabetes	Normal	66	Female
D11	Type	Normal	61	Female
D12	Type	Normal	64	Female

firstly performed a bioinformatics study using miRcode to predict putative binding sites with specific miRNAs. Our results found that MIAT sequence contained the putative binding site of miR-214-3p (Figure 3A). To verify if the putative binding site of miR-214-3p is correct, luciferase assay was performed. The result showed that miR-214-3p transfection could reduce luc-lncRNA-MIAT activity but had no effect on luc-lncRNA-MIAT-mut activity (Figures S1A and S1B). Further, we found that the caspase-1 sequence contained the putative binding site of miR-214-3p (Figure 3B). Luciferase assay demonstrated that miR-214-3p transfection could reduce Luc-CAPS1 activity but had no effect on Luc-CAPS1-mut activity (Figures S1C and S1D). To verify the results, we performed *in-vitro* transfection experiments using primary cardiomyocytes. The results demonstrated that siMIAT treatment significantly increased the level of miR-214-3p, while significantly decreasing the protein expression of caspase-1, as compared to siNC treatment (Figures 3C–3E). Further, we determine if miR-214-3p could regulate CASP1 expression, we transfected primary cardiomyocytes with either miR-214-3p or AMO-miR-214-3p under HG environment, followed by extraction of total RNA for qPCR and extraction of total protein for western blotting. The gene expression of miR-214-3p was verified by qPCR (Figure 3F). Next, we showed that transfection of miR-214-3p significantly decreased gene expression of CASP1, whereas AMO-miR-214-3p treatment significantly increased gene expression of CASP1 (Figure 3G). Similar results were found in protein levels. The results demonstrated that miR-214-3p treatment significantly decreased protein expression of CASP1, whereas AMO-miR-214-3p treatment significantly increased CASP1 production, as compared to corresponding controls (Figure 3H). On the other hand, we performed a confocal microscopy to determine whether miR-214-3p, MIAT, and CASP1 were colocalized in the cytoplasm. The results showed that fluorescein amidites (FAM)-labeled miRNA-214-3p was colocalized with both FAM-labeled MIAT and FAM-labeled CASPA1 (Figures S2A–S2C). In conclusion, these results suggest that MIAT might regulate CASP1 via miR-214-3p. The sequences are listed in Tables 3 and 4.

MIAT regulated pyroptosis in cardiomyocytes via MIAT-miR-214-3p-CASP1 axis

Next, we questioned if the MIAT-miR-214-3p-CASP1 axis played a functional role in pyroptosis in the pathogenesis of DCM. We first measured the expression levels of CASP1, IL-1β, IL-18, and GSDMD, the four markers of pyroptosis, in primary cardiomyocytes under different conditions by western blotting. The results showed that the protein expressions of CASP1, IL-1β, IL-18, and GSDMD were all upregulated after HG treatment, as compared to NG treatment (Figures 4A and 4B). Silencing of MIAT (siMIAT) significantly decreased the protein expression of CASP1, IL-1β, IL-18, and GSDMD as compared to HG treatment plus si-NC treatment (Figures 4A and 4B). Further, we also demonstrated that the protein expression of CASP1, IL-1β, IL-18, and GSDMD were upregulated after transfection with AMO-miR-214-3p in siMIAT cardiomyocytes (siMIAT + AMO-miR-214-3p) as compared to HG + siMIAT + AMO-NC treatment (Figures 4A and 4B). Transmission electron microscopy results demonstrated that MIAT knockdown could recover HG-induced pro-inflammatory damage with a hypertrophic morphology (Figures 4C and 4D). In addition, this recovery in inflammation was destroyed after siMIAT + AMO-miR-214-3p treatment (Figures 4C and 4D). In terms of calcium influx, our results found that HG-induced [Ca^{2+}]$_i$ overload was reduced after either siMIAT treatment or CAPS1 inhibition (Figures 4E and 4F). However, this improvement deteriorated again upon siMIAT + AMO-miR-214-3p treatment (Figures 4E and 4F). As a result, these findings together indicate

Table 2. Data of subjects in the control group

| No.	A prior history of diabetes	Cardiac function	Age	Gender
C1	Without	Normal	66	Female
C2	Without	Normal	61	Male
C3	Without	Normal	65	Female
C4	Without	Normal	66	Female
C5	Without	Normal	62	Female
C6	Without	Normal	68	Male
C7	Without	Normal	64	Male
C8	Without	Normal	68	Male
C9	Without	Normal	68	Male
C10	Without	Normal	66	Female
C11	Without	Normal	64	Female
C12	Without	Normal	62	Male

that MIAT-miR-214-3p-CASP1 axis likely plays a functional role in cardiac pyroptosis. The sequences are listed in Table 3.

Improvement of cardiac function after MIAT knockdown in DM mice

To examine the possibility of MIAT to be developed as a target for DCM treatment, we determined if MIAT knockdown could be a potential strategy in improving cardiac function in DCM. Diabetic mice were successfully established as mentioned in STAR Methods. siMIAT mice were established by injection of lentiviral silenced lncRNA-MIAT (DM + LV-siMIAT) via caudal vein. CASP1 inhibitor was applied to inhibit the effect of pyroptosis *in vivo*. We firstly measured the fasting blood glucose (FBG) of the mice under different groups. The results demonstrated that the FBG of DM + LV-siMIAT mice was significantly decreased as compared to that of DM mice (Figure 5A). Similarly, we found that the FBG of DM + LV-CASP1 I mice was also significantly decreased as compared to that of DM mice (Figure 5A). These results suggest that both MIAT knockdown and CASP1 inhibitor treatment can reduce FBG in diabetic mice. Next, we performed echocardiography to evaluate cardiac function of diabetic mice with different treatments. The results showed that myocardial contractility was partially recovered after DM + LV-siMIAT treatment or DM + CASP-1 inhibitor treatment (Figure 5B) Further, left ventricular ejection fraction (LVEF) and fractional shortening (LVFS) were significantly increased after DM + LV-siMIAT treatment or DM + CASP-1 inhibitor treatment, indicating that MIAT knockdown and CASP1 inhibitor treatment could improve cardiac function of diabetic mice (Figures 5C and 5D). Similar results were also obtained in H&E staining and transmission electron microscopy. H&E staining revealed that high-glucose-induced structural abnormalities including broken fibers, deranged cellular structures, the existence of foci with necrotic myocytes, and the infiltration of inflammatory cells were significantly improved after DM + LV-siMIAT treatment and DM + CASP-1 inhibitor treatment as compared to DM treatment (Figure 5E). The transmission electron microscopy results demonstrated that high-glucose-induced myocardial lesions that consist of of cardiomyocyte swelling, cardiomyocyte degeneration, and inflammatory cell infiltration were substantially ameliorated after DM + LV-siMIAT treatment and DM + CASP-1 inhibitor treatment as compared to DM treatment (Figure 5F).

MIAT knockdown significantly ameliorated cardiac pyroptosis *in vivo*

To study the potential mechanism under this improvement *in vivo*, we performed immunohistochemistry to detect the expressions of CASP1 and IL-1β in diabetic mice. The results showed that high-glucose-induced expressions of CASP1 and IL-1β were significantly decreased upon DM + LV-siMIAT or DM + CASP1 I treatments (Figure 6A). Similarly, the mRNA expressions of CASP1 and IL-1β in mice heart were significantly decreased after MIAT knockdown or CASP1 inhibitor application (Figures 6B–6E). We also verified that knocking down MIAT could increase the expression of miR-214-3p *in vivo*, suggesting that MIAT might target miR-214-3p to regulate the expressions of CASP1 and IL-1β (Figure 6C). We next determined if MIAT was a key regulator in cell pyroptosis *in vivo*. We performed western blotting to determine the expressions of CASP1, IL-1β, IL-18, and GSDMD in mice hearts. The results found that LV-siMIAT or CASP1 I treatment significantly decreased the protein expressions of CASP1, IL-1β, IL-18, and GSDMD as
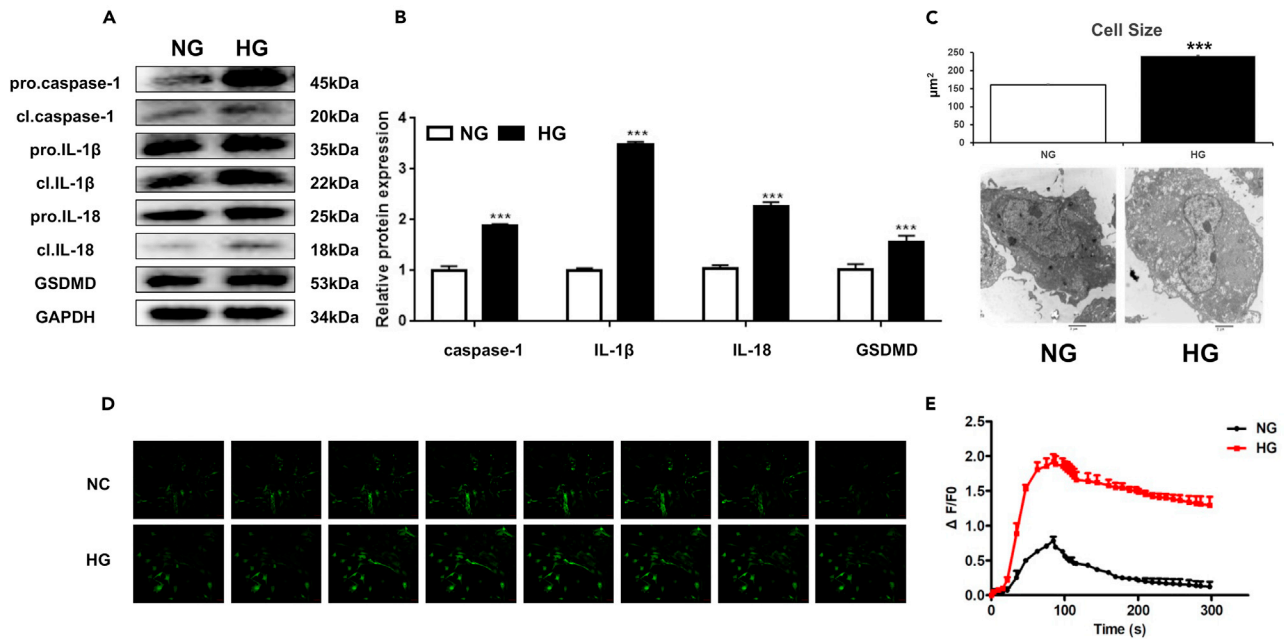
Figure 2. High glucose treatment causes inflammatory damage and calcium overload in cardiomyocytes

(A) The primary cardiomyocyte was treated with either NG or HG for indicated hours. The relative protein expression levels of pro-IL-1β, IL-1β, pro-CASP1, CASP1, pro-IL-18, IL-18, and GSDMD in cardiomyocytes were detected by western blotting.

(B) Densitometry analysis was performed and demonstrated as fold change.

(C) Representative transmission electron microscopy images. Scale bar: 2 μm, three different sections were captured, and the area of each cell were calculated. ***$p < 0.001$.

(D) The baseline and peak fluorescence in primary human cardiomyocytes with either NG or HG treatment were captured via confocal microscopy.

(E) The baseline and peak fluorescence intensity were demonstrated as a line chart. Scale bar: 20 μm. n = 5 for each experiment. All experiments are performed at least 3 times.

compared to DM treatment, suggesting that MIAT was responsible for regulate cell pyroptosis *in vivo* (Figures 6F and 6G). Finally, we applied patch clamping to measure L-type calcium ($I_{Ca,L}$) changes. The results showed DM-induced $I_{Ca,L}$ upregulation fell back after DM + LV-siMIAT or DM + CASP1 I treatment, suggesting that DM-induced calcium overload could be reduced by either MIAT knockdown or inhibition of CASP1 (Figure 6H). Taken together, these results together indicate that MIAT/miR-214-3p/CASP1 pathway was responsible for cardiac pyroptosis in diabetic mice.
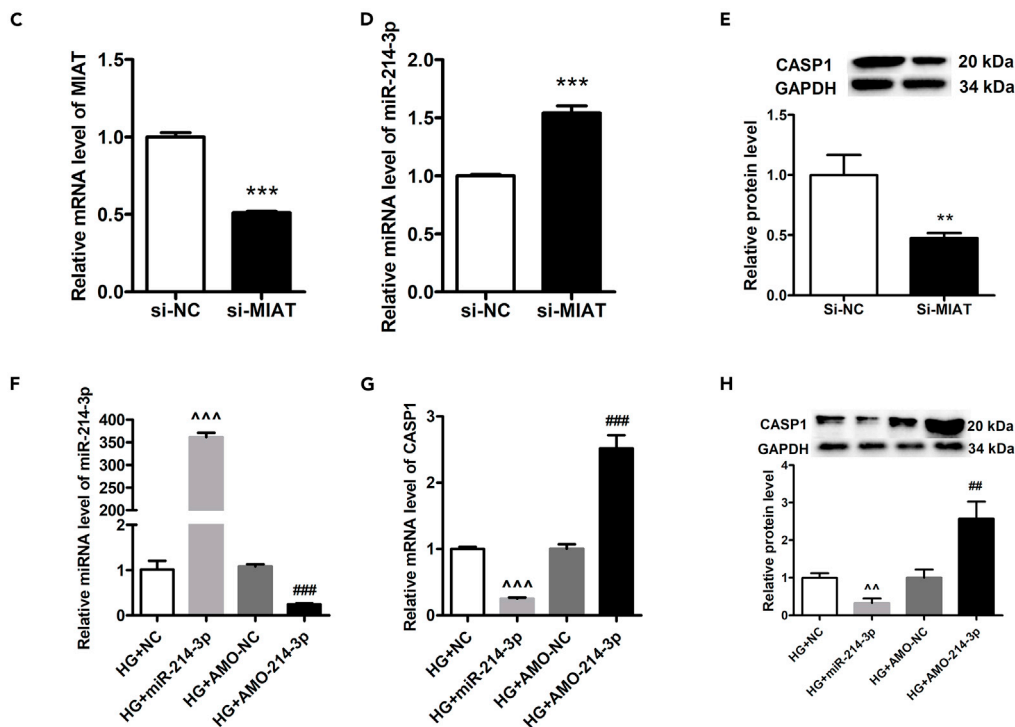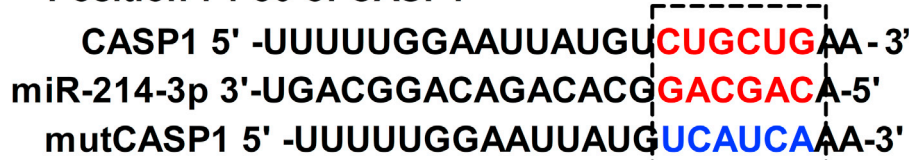
DISCUSSION

As a type of eukaryotic transcription products, lncRNAs participate in a diversity of biological processes via various mechanisms of action. Recently, it was found that they also played an important role in the pathogenesis of many diseases. In the past years, the relationship between lncRNAs and DCM has also been reported. For examples, lncRNA MEG3 promoted high glucose-induced cardiomyocyte apoptosis (Chen et al., 2019); LncRNA Crnde reversed myocardial fibrosis in DCM by negative feedback regulation of Smad3. In our study, we found that the expression of MIAT was significantly increased under high-glucose conditions. Further, both *in vitro* and *in vivo* study supported that knocking down of MIAT significantly improved cardiomyocyte contractility. These findings reveal that MIAT is a key factor induced by abnormal glucose metabolism, contributing to the onset of diabetic cardiomyopathy.

Because MIAT played an important role in regulating cardiomyocyte pyroptosis, contributing to the development of DCM, our study further studied the detailed mechanism by which MIAT regulated host pyroptosis. LncRNAs could act as miRNA sponges, regulating miRNAs available for binding their target mRNAs (Yan et al., 2015). For instance, MIAT regulated microvascular relaxation and contraction by functioning as a competing endogenous RNA (Yan et al., 2015); MIAT promoted gastric cancer growth and metastasis by regulation of the miR-141/DDX5 pathway (Sha et al., 2018). In our study, we revealed that MIAT could

A   **Position 5265-6124 of MIAT**

MIAT 5' -GACTCCTGTGTGTGT CUGCUGA - 3'
miR-214-3p 3'-UGACGGACAGACACG GACGACA-5'
mutMIAT 5' -GACTCCTGTGTGTGTC TGATGAA-3'

B   **Position 74-80 of CASP1**

CASP1 5' -UUUUUGGAAUUAUGU CUGCUGAA - 3'
miR-214-3p 3'-UGACGGACAGACACG GACGACA-5'
mutCASP1 5' -UUUUUGGAAUUAUG UCAUCAAA-3'

Figure 3. Verification of binding between MIAT and miR-214-3p

(A) The binding sites between MIAT and miR-214-3p, as predicted by the bioinformatic assay, were shown in the top panel.

(B) The binding sites between miR-214-3p and CASP1 were shown in the bottom panel.

(C) The gene expression levels of MIAT between MIAT knockdown group and control group were determined by qPCR.

(D) The gene expressions of miR-214-3p between MIAT knockdown group and control group were determined by qPCR.

(E) The relative protein expression levels of CASP1 between MIAT knockdown group and control group were detected by western blotting, and densitometry analysis was performed and demonstrated as fold change, normalized to GAPDH.

(F) HG-induced primary cardiomyocytes were transfected with either miR-214-3p or AMO-miR-214-3p. The expression of miR-214-3p was detected by qRT-PCR among different groups, and si-NC and AMO-NC were set as negative control to miR-214-3p or AMO-miR-214-3p, respectively.

(G) HG-induced primary cardiomyocytes were transfected with either miR-214-3p or AMO-miR-214-3p. The expression of CASP1 was detected by qRT-PCR among different groups, and si-NC and AMO-NC were set as negative control to miR-214-3p or AMO-miR-214-3p, respectively.

(H) HG-induced primary cardiomyocytes were transfected with either miR-214-3p or AMO-miR-214-3p. The expression of CASP1 were detected by western blotting among different groups, and si-NC and AMO-NC were set as negative control to miR-214-3p or AMO-miR-214-3p, respectively, and densitometry analysis was performed and demonstrated as fold change, normalized to GAPDH. All experiments were performed at least 3 times. **$p < 0.01$, ***$p < 0.001$ versus si-NC; ^^$p < 0.01$, ^^^$p < 0.001$ versus HG + NC; ##$p < 0.01$, ###$p < 0.001$ versus HG + AMO-NC.

Table 3. Interfering RNA sequence

Interfering		RNA sequence
miR-214-3p mimic	Forward	5′-ACAGCAGGCACAGAGACCGGCAGU-3′
	Reverse	3′-UGUCGUCCGUGUCUGUGUCCGUCA-5′
miR-214-3p inhibitor		5′-mAmCmUmGmCmCmUmGmUmCmUmGmU mGmCmCmUmGmCmUmGmUmGmU-3′

specifically target miR-214-3p, sponging the effect of miR-214-3p on silencing CASP1, contributing to the onset of pyroptosis.

Pyroptosis is an inflammatory process associated with cell death. Accumulated studies indicated that pyroptosis played an important role in DCM (Li et al., 2014; Luo et al., 2017; Yang et al., 2019b). In our study, the expressions of pyroptosis-associated factors GSDMD, CASP1, and IL-1β were significantly elevated in HG-induced cardiomyocytes, whereas their expressions were downregulated after silencing MIAT. This result suggests that silencing MIAT can inhibit pyroptosis. Although CASP1 inhibitor had the same effect as MIAT silencing, knocking down of MIAT manifested a stronger effect on inhibition of CASP1 activity in cardiomyocytes and diabetic mice as compared to CASP1 inhibitor. These results suggest that MIAT is probably a more effective target than CASP1 for drug development. This hypothesis was also supported by other studies. Fu et al. reported that silencing of MIAT sensitizes lung cancer cells to gefitinib by epigenetically regulating miR-34a (Fu et al., 2018). Zeng et al. demonstrated that cardiomyocyte autophagy was enhanced by berberine-induced MIAT knockdown, which further contributed to the improved cardiomyocyte contractility (Zeng et al., 2019). Therefore, development of a small molecule which can specifically target MIAT could be our next aim.

So far, there have been few reports of the MIAT effects on Ca^{2+} ion channels. Because dysfunction of Ca^{2+} ion channel was highly associated with DCM cardiomyocytes, we speculated that MIAT might work as an endogenous mediator responsible for activation of Ca^{2+}/calmodulin-dependent kinase PNCK, which in turn phosphorylated IκBα and triggered calcium-dependent nuclear factor κB (NF-κB) activation. Another possibility was that MIAT might target SERCA, a sarcoplasmic reticulum Ca^{2+} ATPase, resulting in the Ca^{2+} overload.

In conclusion, our study first reported that MIAT regulated cardiomyocyte pyroptosis via sponging miR-214-3p. Disruption of MIAT-miR-214-3p-CASP1 axis was a potential strategy for attenuating high-glucose-induced DCM.

Table 4. PCR primer sequence

| Primer		RNA sequence (5′-3′)	Product length (bp)
U6	Forward	CTCGCTTCGGCAGCACATATACT	95
	Reverse	ACGCTTCACGAATTTGCGTGTC	
MIAT	Forward	TGGAACAAGTCACGCTCGATT	150
	Reverse	GGTATCCCAAGGAATGAAGTCTGT	
CASP1	Forward	ACACGTCTTGCCCTCATTATCT	365
	Reverse	ATAACCTTGGGCTTGTCTTTCA	
IL-1β	Forward	CCCTGCAGCTGGAGAGTGTGG	153
	Reverse	TGTGCTCTGCTTGAGAGGTGCT	
GAPDH	Forward	ATCACTGCCACCCAGAAGAC	211
	Reverse	TTTCTAGACGGCAGGTCAGG	
miR-214-3p		miRNA quantification: Bulge-loop™ miRNA qRT-PCR primer sets (one RT primer and a pair of qPCR primer for each set) specific for miR-214-3p are designed by RiboBio (Guangzhou, China) (Bulge-Loop™ miR-214-3p Reverse Primer: No. ssD089261711, Bulge-Loop™ miR-214-3p Forward Primer: No. ssD809230935, Bulge-Loop™ miR-214-3p RT Primer: No. ssD809230243)	
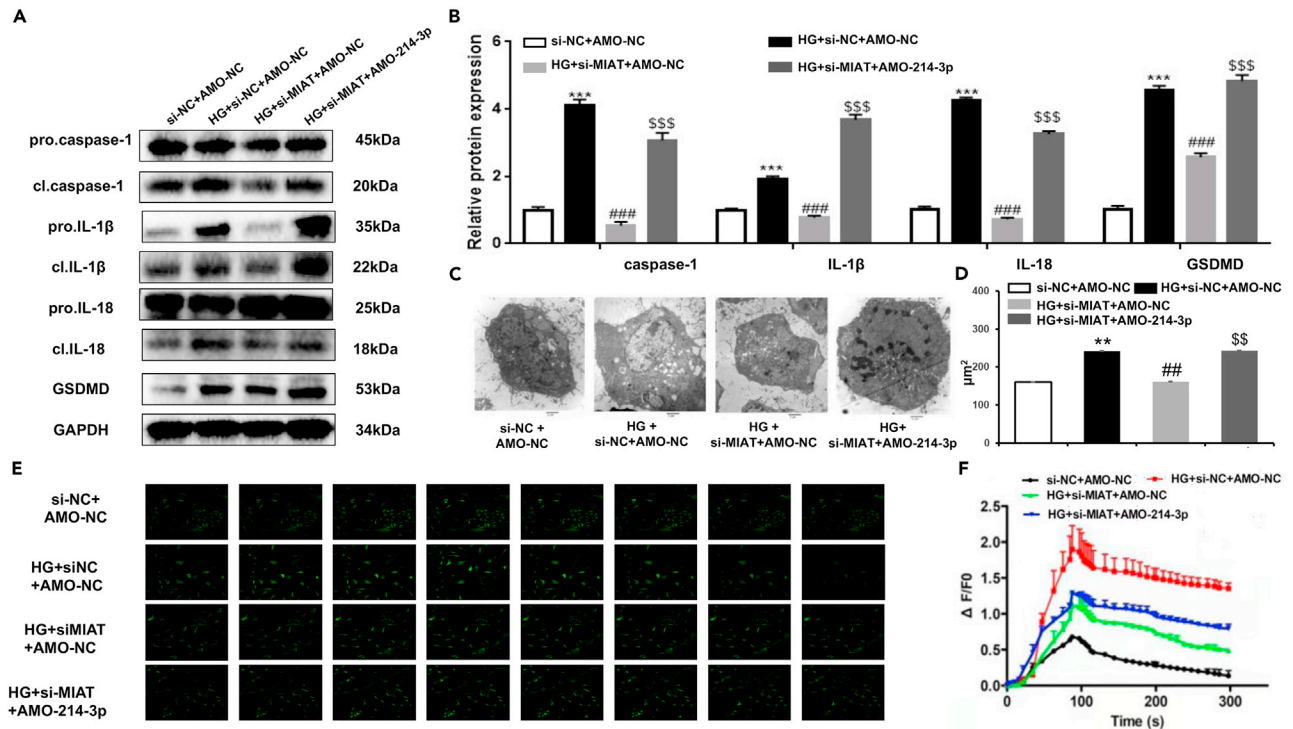
Figure 4. MIAT regulated pyroptosis in cardiomyocytes via MIAT-miR-214-3p-CASP1 axis

(A and B) Primary cardiomyocytes treated with si-NC + AMO-NC, HG + si-NC + AMO-NC, HG + si-MIAT + AMO-NC, HG + si-NC + AMO-miR-214-3p, respectively, were harvested for western blotting. The protein expression levels of CASP1, IL-1β, IL-18, and GSDMD were detected by immunofluorescence. Densitometry analysis was performed and demonstrated as fold change, normalized to GAPDH.

(C and D) Representative transmission electron microscopy images of primary cardiomyocytes with indicated treatments. Scale bar: 2 μm, three different sections were captured, and the area of each cell was calculated.

(E) The images of fluorescence intensity of $[Ca^{2+}]_i$ in primary cardiomyocytes with each indicated treatment was captured by confocal microscopy, and $[Ca^{2+}]_i$ was labeled by arrows.

(F) Fluorescence measurement of $[Ca^{2+}]_i$ in primary cardiomyocytes with indicated treatments. The baseline and peak fluorescence intensity were demonstrated as a line chart. Scale bar: 20 μm. All experiments are performed at least 3 times. $**p < 0.01$, $***p < 0.001$ versus si-NC + AMO-NC; $^{##}p < 0.01$, $^{###}p < 0.001$ versus HG + si-NC + AMO-NC; $^{\$\$}p < 0.01$, $^{\$\$\$}p < 0.001$ versus HG + si-MIAT + AMO-NC.

STAR★METHODS

Detailed methods are provided in the online version of this paper and include the following:

- KEY RESOURCES TABLE
- RESOURCE AVAILABILITY
  - Lead contact
  - Materials availability
  - Data and code availability
- EXPERIMENTAL MODEL AND SUBJECT DETAILS
  - For human studies
  - For animal studies
  - For cell lines and primary cultures
- METHOD DETAILS
  - Samples from patients
  - Establishment of the diabetic mice model
  - Echocardiography
  - Transmission electron microscopy
  - Histology and immunohistochemistry
  - Cell culture and transfection
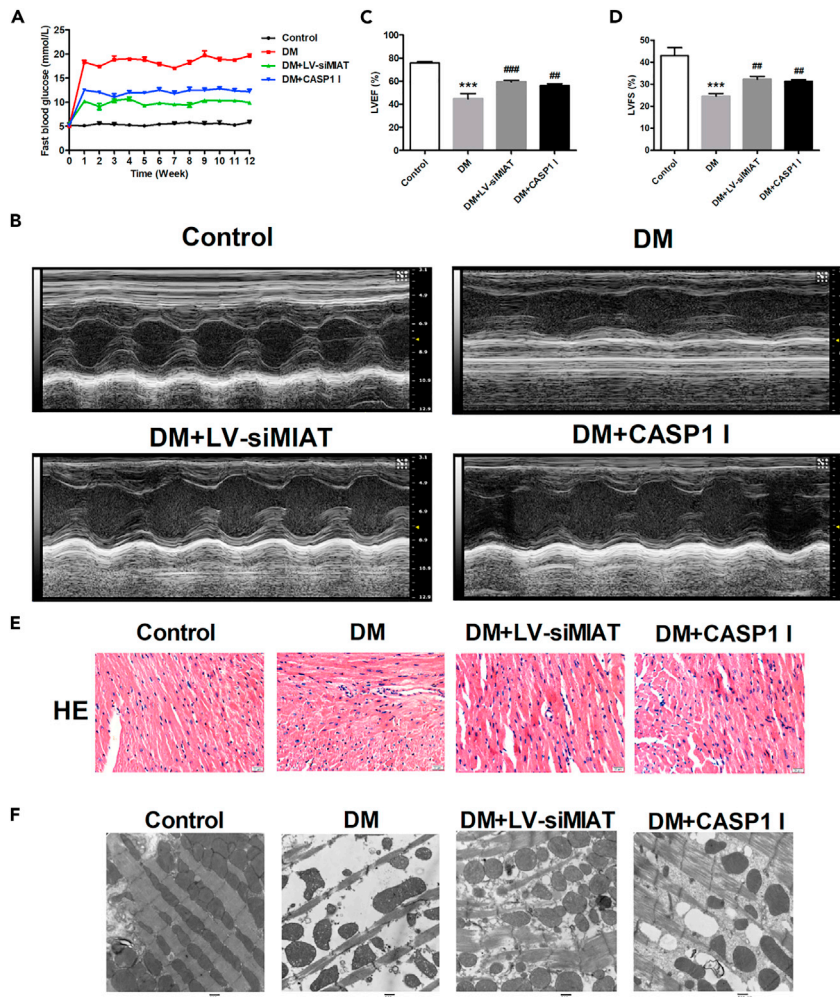
Figure 5. Improvement of cardiac function after MIAT knockdown in DM mice

(A) Mice with indicated treatments were processed for fast blood glucose testing once a week. Line charts of fast blood glucose levels were demonstrated.

(B) Mice with indicated treatments were processed for echocardiography examination. Representative images of mice hearts were visualized by the Vevo 1100 high resolution imaging system.

(C) Left ventricular ejection fraction (LVEF) of mice with indicated treatment was evaluated by the Vevo 1100 high resolution imaging system and plotted.

(D) Left ventricular fractional shortening (LVFS) of mice with indicated treatment was evaluated by the Vevo 1100 high resolution imaging system and plotted.
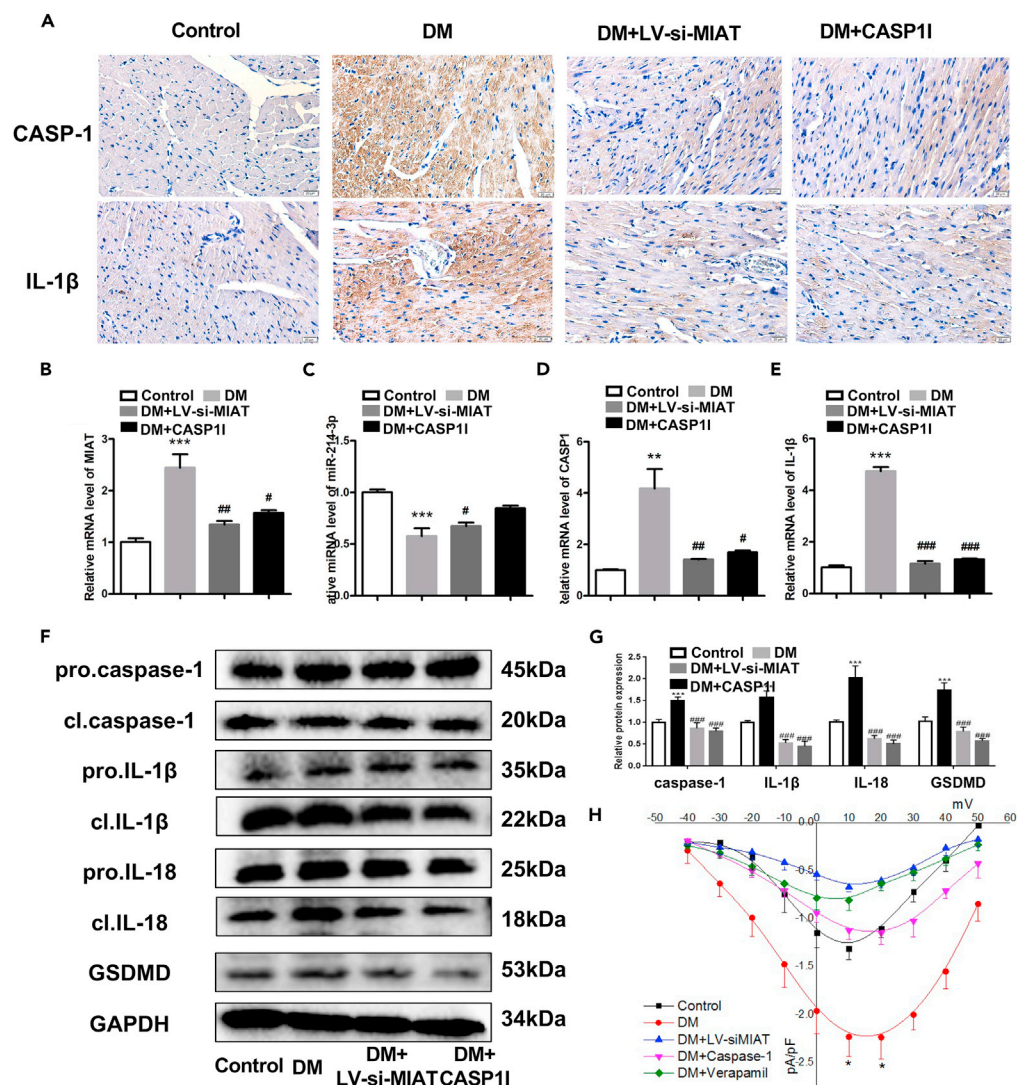
(E) Representative H&E images of mice with indicated treatment were demonstrated at ×40.

(F) Representative transmission electron microscopy images of mice with indicated treatment. Scale bar: 500 nm. n = 5 for each experiment. ***$p < 0.001$ versus the control group; ##$p < 0.01$ versus DM, ###$p < 0.001$ versus DM.

○ RNA isolation and quantitative real-time -PCR (qRT-PCR)
○ Western blotting
○ Measurement of $[Ca^{2+}]_i$ in cardiomyocytes
○ Whole-cell patch clamp method
● QUANTIFICATION AND STATISTICAL ANALYSIS

SUPPLEMENTAL INFORMATION

Supplemental information can be found online at https://doi.org/10.1016/j.isci.2021.103518.

Figure 6. MIAT knockdown significantly ameliorated cardiac pyroptosis *in vivo*

(A) Representative immunohistochemistry heart images of CASP1 and IL-1β in mice with indicated treatments.

(B–E) The relative gene expression levels of MIAT (B), miR-214-3p (C), CASP1 (D), and IL-1β (E) in control, DM, DM + LV-siMIAT, and DM + CASP1 I groups.

(F) The relative protein expression levels of CASP1, IL-1β, IL-18, and GSDMD in control, DM, DM + LV-siMIAT, and DM + CASP1 I groups were detected by western blotting. Densitometry analysis was performed and demonstrated as fold change, normalized to GAPDH.

(G) is Densitometry analysis was performed and demonstrated as fold change, normalized to GAPDH.

(H) I$_{Ca,L}$ was detected by patch clamping The baseline and peak fluorescence intensity were demonstrated as line charts. Scale bar: 20 μm. n = 5 for each experiment. Treatment using verapamil (20umol/L) to block calcium channel was used as a positive control **p $<$ 0.01, ***p $<$ 0.001 versus the control group. #p $<$ 0.05, ##p $<$ 0.01 versus DM, ###p $<$ 0.001 versus DM.

REFERENCES

Bulani, Y., and Sharma, S.S. (2017). Argatroban attenuates diabetic cardiomyopathy in rats by reducing fibrosis, inflammation, apoptosis, and protease-activated receptor expression. Cardiovasc. Drugs Ther. 31, 255–267. https://doi.org/10.1007/s10557-017-6732-3.

Chen, Y., Zhang, Z., Zhu, D., Zhao, W., and Li, F. (2019). Long non-coding RNA MEG3 serves as a ceRNA for microRNA-145 to induce apoptosis of AC16 cardiomyocytes under high glucose condition. Biosci. Rep. 39. https://doi.org/10.1042/BSR20190444.

Fu, Y.F., Li, C.Y., Luo, Y.W., Li, L., Liu, J., and Gui, R. (2018). Silencing of long non-coding RNA MIAT sensitizes lung cancer cells to gefitinib by epigenetically regulating miR-34a. Front Pharmacol. https://doi.org/10.3389/fphar.2018.00082.

Knauss, J.L., and Sun, T. (2013). Regulatory mechanisms of long noncoding RNAs in vertebrate central nervous system development and function. Neuroscience 235, 200–214. https://doi.org/10.1016/j.neuroscience.2013.01.022.

Lee, C., and Kikyo, N. (2012). Strategies to identify long noncoding RNAs involved in gene regulation. Cell Biosci. 2, 37. https://doi.org/10.1186/2045-3701-2-37.

Li, X., Du, N., Zhang, Q., Li, J., Chen, X., Liu, X., Hu, Y., Qin, W., Shen, N., Xu, C., et al. (2014). MicroRNA-30d regulates cardiomyocyte pyroptosis by directly targeting foxo3a in diabetic cardiomyopathy. Cell Death Dis. 5, e1479. https://doi.org/10.1038/cddis.2014.430.

Liu, Y., Wang, T., Zhang, M., Chen, P., and Yu, Y. (2019). Down-regulation of myocardial infarction associated transcript 1 improves myocardial ischemia-reperfusion injury in aged diabetic rats by inhibition of activation of NF-kappaB signaling pathway. Chem. Biol. Interact. 300, 111–122. https://doi.org/10.1016/j.cbi.2019.01.001.

Luo, B., Huang, F., Liu, Y., Liang, Y., Wei, Z., Ke, H., Zeng, Z., Huang, W., and He, Y. (2017). NLRP3 inflammasome as a molecular marker in diabetic cardiomyopathy. Front. Physiol. 8, 519. https://doi.org/10.3389/fphys.2017.00519.

Mohanty, R.R., and Das, S. (2017). Inhaled insulin - current direction of insulin research. J. Clin. Diagn. Res. 11, OE01–OE02. https://doi.org/10.7860/JCDR/2017/23626.9732.

Niu, Z.S., Niu, X.J., and Wang, W.H. (2017). Long non-coding RNAs in hepatocellular carcinoma: potential roles and clinical implications. World J. Gastroenterol. 23, 5860–5874. https://doi.org/10.3748/wjg.v23.i32.5860.

Novikova, I.V., Hennelly, S.P., and Sanbonmatsu, K.Y. (2012). Sizing up long non-coding RNAs: do lncRNAs have secondary and tertiary structure? Bioarchitecture 2, 189–199. https://doi.org/10.4161/bioa.22592.

Peng, X., Gralinski, L., Armour, C.D., Ferris, M.T., Thomas, M.J., Proll, S., Bradel-Tretheway, B.G., Korth, M.J., Castle, J.C., Biery, M.C., et al. (2010). Unique signatures of long noncoding RNA expression in response to virus infection and altered innate immune signaling. mBio 1. https://doi.org/10.1128/mBio.00206-10.

Qi, Y., Wu, H., Mai, C., Lin, H., Shen, J., Zhang, X., Gao, Y., Mao, Y., and Xie, X. (2020). LncRNA-MIAT-mediated miR-214-3p silencing is responsible for IL-17 production and cardiac fibrosis in diabetic cardiomyopathy. Front. Cel. Dev. Biol. 8, 243. https://doi.org/10.3389/fcell.2020.00243.

Ruhl, S., Shkarina, K., Demarco, B., Heilig, R., Santos, J.C., and Broz, P. (2018). ESCRT-dependent membrane repair negatively regulates pyroptosis downstream of GSDMD activation. Science 362, 956–960. https://doi.org/10.1126/science.aar7607.

Schneider, C.A., Rasband, W.S., and Eliceiri, K.W. (2012). NIH Image to ImageJ: 25 years of image analysis. Nat. Methods 9, 671–675. https://doi.org/10.1038/nmeth.2089.

Sha, M., Lin, M., Wang, J., Ye, J., Xu, J., Xu, N., and Huang, J. (2018). Long non-coding RNA MIAT promotes gastric cancer growth and metastasis through regulation of miR-141/DDX5 pathway. J. Exp. Clin. Cancer Res. 37, 58. https://doi.org/10.1186/s13046-018-0725-3.

Yan, B., Yao, J., Liu, J.Y., Li, X.M., Wang, X.Q., Li, Y.J., Tao, Z.F., Song, Y.C., Chen, Q., and Jiang, Q. (2015). lncRNA-MIAT regulates microvascular dysfunction by functioning as a competing endogenous RNA. Circ. Res. 116, 1143–1156. https://doi.org/10.1161/CIRCRESAHA.116.305510.

Yang, F., Qin, Y., Lv, J., Wang, Y., Che, H., Chen, X., Jiang, Y., Li, A., Sun, X., Yue, E., et al. (2018). Silencing long non-coding RNA Kcnq1ot1 alleviates pyroptosis and fibrosis in diabetic cardiomyopathy. Cell Death Dis. 9, 1000. https://doi.org/10.1038/s41419-018-1029-4.

Yang, F., Li, A., Qin, Y., Che, H., Wang, Y., Lv, J., Li, Y., Li, H., Yue, E., Ding, X., et al. (2019a). A novel circular RNA mediates pyroptosis of diabetic cardiomyopathy by functioning as a competing endogenous RNA. Mol. Ther. Nucleic Acids 17, 636–643. https://doi.org/10.1016/j.omtn.2019.06.026.

Yang, F., Qin, Y., Wang, Y., Meng, S., Xian, H., Che, H., Lv, J., Li, Y., Yu, Y., Bai, Y., and Wang, L. (2019b). Metformin inhibits the NLRP3 inflammasome via AMPK/mTOR-dependent effects in diabetic cardiomyopathy. Int. J. Biol. Sci. *15*, 1010–1019. https://doi.org/10.7150/ijbs.29680.

Zeng, Z., Pan, Y., Wu, W., Li, L., Wu, Z.J., Zhang, Y.G., Deng, B., Wei, S.Y., Zhang, W.W., Lin, F.X., and Song, Y.Z. (2019). Myocardial hypertrophy is improved with berberine treatment via long non-coding RNA MIAT-mediated autophagy. J. Pharm. Pharmacol. *71*, 1822–1831. Epub 2019 Oct 14. https://doi.org/10.1111/jphp.13170.

Zhou, X., Zhang, W., Jin, M., Chen, J., Xu, W., and Kong, X. (2017). lncRNA MIAT functions as a competing endogenous RNA to upregulate DAPK2 by sponging miR-22-3p in diabetic cardiomyopathy. Cell Death Dis. *8*, e2929. https://doi.org/10.1038/cddis.2017.321.

STAR★METHODS

KEY RESOURCES TABLE

REAGENT or RESOURCE	SOURCE	IDENTIFIER
Antibodies		
Caspase-1 Rabbit pAb (A0964)	ABclonal	Cat#AB_2757485
IL1β Rabbit pAb (A16288)	ABclonal	Cat#AB_2769945
IL18 Rabbit pAb (A20473)	ABclonal	Cat#A20473
GSDMD Rabbit mAb	ABclonal	Cat#A20728
GAPDH Rabbit mAb (A19056)	ABclonal	Cat#AB_2862549
Bacterial and virus strains		
lentiviral shRNA for MIAT	Gene Pharma	N/A
Biological samples		
Healthy human serum sample	General Hospital of Western Theater Command	Cat#CDZYY2017KY-108
Diabetic human serum sample	General Hospital of Western Theater Command	Cat#CDZYY2017KY-108
Chemicals, peptides, and recombinant proteins		
HEPES	VETEC	Cat#V900477
Glucose	VETEC	Cat#V900392
$NaH_2PO_4 \cdot 2H_2O$	VETEC	Cat#V900060
NaOH	VETEC	Cat#V900797
CaCl2	VETEC	Cat#V900266
CsCl	VETEC	Cat#V900481
TEACl	VETEC	Cat#V900405
L-Glutamic acid	VETEC	Cat#V900408
KH_2PO_4	VETEC	Cat#V900041
EGTA	VETEC	Cat#03779
Z-Asp(OtBu)-OH	VETEC	Cat#02378
CsOH	SIGMA-ALDRICH	Cat#232041
Alexa Fluor™ 488 Phalloidin	Invitrogen	Cat#A12379
NaCl	VETEC	Cat#V900058
KCl	VETEC	Cat#V900068
$MgCl_2 \cdot 6H_2O$	VETEC	Cat#V900020
Pluronic F-127	Invitrogen	Cat#P3000MP
Critical commercial assays		
X-treme GENE siRNA transfection reagent	Roche	4476093001
HE stain kit	Solarbio	G1120
SYBR Green I	Toyobo	QPK-201
Deposited data		
Original western blot images	Mendeley	https://doi.org/10.17632/cc8bb3bthw.1
Experimental models: Cell lines		
Mouse: primary cardiomyocytes cell culture	Laboratory of the General Hospital of Western Theater Command	N/A

Continued

REAGENT or RESOURCE	SOURCE	IDENTIFIER
Experimental models: Organisms/strains		
Mouse: C57BL/6	Liaoning Changsheng Biotechnology Co., Ltd.	Cat#76219
Oligonucleotides		
miR-214-3p		
Forward Primer: No. ssD809230935, Bulge-Loop™ miR-214-3p RT Primer: No. ssD809230243	RIOBIO	N/A
Bulge-Loop™ miR-214-3p Reverse Primer: No. ssD089261711, Bulge-Loop™ miR-214-3p		
Caspase-1		
Forward Primer: 5′-ACACGTCTTGC CCTCATTATCT-3′	Gene Tools	N/A
Reverse Primer: 5′-ATAACCTTGGGCTT GTCTTTCA-3′		
IL-1β		
Forward Primer: 5′-CCCTGCAGCTGGAG AGTGTGG-3′	Gene Tools	N/A
Reverse Primer: 5′-TGTGCTCTGCTTGAGA GGTGCT-3′		
MIAT		
Forward Primer: 5′-TGGAACAAGTCACG CTCGATT-3′	Gene Tools	N/A
Reverse Primer: 5′- GGTATCCCAAGGAATG AAGTCTGT -3′		
miR-214-3p mimic		
Forward Primer: 5′-ACAGCAGGCACAGA GACCGGCAGU-3′	RIOBIO	N/A
Reverse Primer: 3′-UGUCGUCCGUGUCUG UGUCCGUCA-5′		
GAPDH		
Forward Primer: 5′-ATCACTGCCACCCA GAAGAC-3′	Gene Tools	N/A
Reverse Primer: 5′-TTTCTAGACGGCAG GTCAGG-3′		
U6		
Forward Primer: 5′-CTCGCTTCGGCAGCA CATATACT-3′	Gene Tools	N/A
Reverse Primer: 5′-ACGCTTCACGAATTTG CGTGTC-3′		
Software and algorithms		
ImageJ	Schneider et al., 2012	https://imagej.nih.gov/ij/

RESOURCE AVAILABILITY

Lead contact

Further information and requests for resources and reagents should be directed to and will be fulfilled by the lead contact, Wenjing Xiao (xwj-4321@163.com).

Materials availability

This study did not generate new unique reagents.

Data and code availability

Original western blot images have been deposited at Mendeley and are publicly available as of the date of publication. The DOI is listed in the key resources table. Microscopy data reported in this paper will be shared by the lead contact upon request.

Any additional information required to reanalyze the data reported in this paper is available from the lead contact upon request.

EXPERIMENTAL MODEL AND SUBJECT DETAILS

For human studies

Serum samples of 12 diabetic and 12 healthy controls were collected at the General Hospital of Western Theater Command (Chengdu, China) from December 2017 to December 2019. None of patients had a history of hypertension, coronary artery disease or other heart diseases. Informed consent was signed by all patients who participated in the study. This study was performed in accordance with clinical study protocols and the principles of the Declaration of Helsinki (modified 2000), and approved by the Ethics Committee of the General Hospital of Western Theater Command of PLA (CDZYY2017KY-108).

Inclusion criteria: (1) Adults who had more than 10 years of diabetes. (2) Patients who underwent standardized treatment according to the guideline. Exclusion criteria: (1) Complicated with hypertension or organic cardiopathy. Groupings: 1. diabetes group; 2. Control group.

The detail medical records of subjects have been uploaded as attachments and basic data as following table (Tables 1 and 2).

For animal studies

The study was approved by the Animal Research Ethics Committee of the General Hospital of Western Theater Command (Chengdu, China) and complied with the Guidelines for Animal Experiments on Laboratory Animals. Male C57BL/6 mice weighing 18-20 g from Liaoning Changsheng Biotechnology Co., Ltd. (China; license no. 76219) were given adaptive food for a week and randomly divided into four groups.

For cell lines and primary cultures

C57BL/6 mice aged 1-3 days (male: female 1:1) were killed and soaked in 75% alcohol for 30s for disinfection. The left hand pinched the back of the suckling mice, and the right hand used sterile surgical scissors to snip the skin and sternum, gently squeezed then quickly taken out the heart of suckling mice with sterile tweezers. Place the heart in a plate with PBS buffer on ice. Then drain the blood, remove the atrium, blood vessels and surrounding connective tissue, and rinse the remaining ventricular tissue with pre-cold PBS for 3 times. Put the washed ventricular tissue into BD tube, cut it into 1-3mm pieces, and add trypsin-collagenase II buffer (60 mg trypsin + 40 mg collagenase II, dissolved to 100 mL with 1×ADS solution.) about twice the volume of the tissue preheated to 37°C. The BD tube was shake at 37°C for about 10 min, absorb the supernatant and mix it with 8 mL DMEM medium (Contains 15% calf serum) to terminate the digestion process, and store it in a 4°C refrigerator. Repeat the above operations until the suckling mice heart is completely digested. The harvested cell suspension was evenly mixed and filtered through a 200-mesh sterile filter screen. After filtration, evenly divide into 15mL centrifuge tube, 1000 rpm, centrifuge at 4°C for 8 min, discard the supernatant, resuspended with DMEM medium (Contains 10% calf serum) and carefully collect the cells in the culture bottle, then culture the cells at 5% CO_2 and 37°C for 2 hours. Myocardial fibroblasts adhered to the wall and then carefully sucked out the suspended myocardial cells. Cardiomyocytes were resuspended in high glucose medium (containing 25 mM glucose) or normal medium (5.5 mm), inoculating into 6-well plates, and still cultured at 5% CO_2 and 37°C for follow-up experiments.

METHOD DETAILS

Samples from patients

Samples of 12 diabetic patients and 12 healthy controls were collected at the General Hospital of Western Theater Command (Chengdu, China) from December 2017 to December 2019. None of patients had a history of hypertension, coronary artery disease or other heart diseases. Informed consent was signed by all patients who participated in the study. This study was performed in accordance with clinical study protocols and the principles of the Declaration of Helsinki (modified 2000), and approved by the Ethics Committee of the General Hospital of Western Theater Command (CDZYY2017KY-108).

Establishment of the diabetic mice model

The study was approved by the Animal Research Ethics Committee of the General Hospital of Western Theater Command (Chengdu, China) and complied with the Guidelines for Animal Experiments on Laboratory Animals. Male C57BL/6 mice weighing 18-20 g from Liaoning Changsheng Biotechnology Co., Ltd. (China; license no. 76219) were given adaptive food for a week and randomly divided into four groups, including a control group (Control), diabetic group (DM), diabetes combined with MIAT lentivirus shRNA group (DM + MIAT-shRNA) and diabetes combined with CASP1 inhibitor group (DM + CASP1). Mice were administered 150 mg/kg streptozotocin (STZ, Sigma, St. Louis, MO, USA) in citrate buffer (pH = 4.6) once and blood glucose were measured once week by Contour blood glucose meter (Roche, Basel, Switzerland). The diabetes model was confirmed as the blood glucose value of the mice was above 11.1 mmol/L. Subsequently, diabetic mice were treated with MIAT lentivirus or CASP1 inhibitor. The lentiviral shRNA for MIAT was purchased from Gene Pharma Technology Co., Ltd. (Shanghai, China); l × 10^9 TU lentiviral shRNA was dissolved in 50 μL saline and intravenously injected into diabetic mice. Mice in the DM + CASP1 I group were given 0.1 mg/kg of the CASP1 inhibitor Ac-YVAD-CMK (Cayman Chemical, MI, USA) daily by intraperitoneal injection. All mice were maintained for 12 weeks, and inhalation of CO_2 (20% of the displacement volume per min) was used for euthanasia (n = 5).

Echocardiography

After 12 weeks of management, Vevo® 1100 high resolution imaging system (Visual Sonics, Toronto, Canada) was used to perform echocardiography and measure left ventricular ejection fraction (EF) and fractional shortening (FS). The technical information refers to https://www.visualsonics.com/product/imaging-systems/vevo-1100. All the ultrasonic operators are attending doctors with more than 5 years of working experience.

Transmission electron microscopy

Ventricular anterior wall of the mice was collected, followed by fixation in 2.5% glutaraldehyde with sodium cacodylate buffer (pH 7.4), and diced into small pieces, postfixed in 1% osmium tetroxide, and embedded in Epon 812. Thin sections from selected tissue blocks were cut with an LKB Ultramicrotome (BZ10118513, MS, USA), stained with uranyl acetate and lead citrate. The slices were viewed using a transmission electron microscope (JEM-1230, JEOL Ltd., Tokyo, Japan).

Histology and immunohistochemistry

Left ventricular samples from mice were cut into 4-μm thick sections, deparaffinized with xylene and rehydrated through graded ethanol (0012036210, Fuyu Chemistry Co., Ltd.) washes. Then the sections were immersed in sodium citrate antigen retrieval solution (C1032, Solarbio, Beijing, China) at 100°C for 5 min, and then were cooled to room temperature. To detect the expression of CASP1 and IL-1β in mice tissue, sections were stained with primary antibody against CASP1 (1:200; A0964, ABclonal, MA, USA) and IL-1β (1:200; A16737, ABclonal, MA, USA) overnight at 4°C. The sections were then washed three times with phosphate buffered saline (PBS) and incubated with secondary antibody at room temperature for 1 hour. Slides were rinsed in PBS and were visualised by using a DAKO EnVision Detection system (Fuzhou MXB® Biotechnology Development Co., Ltd.). Image-Pro Plus 6.0 was used to quantify data.

Cell culture and transfection

Primary cardiomyocytes were extracted from the hearts of C57BL/6 mice within 3 days of born. Cells were incubated with 5.5 mM glucose (NG) or 25 mM glucose (HG) for 24 hours in Dulbecco's modified Eagle's medium (DMEM, Biological Industries, Beit-Haemek, Israel) supplemented with 10% fetal bovine serum

(Biological Industries, Beit-Haemek, Israel) at 37°C and 5% CO_2. Primary cardiomyocytes in HG group were untreated or treated with 100 µM CASP1 inhibitor Ac-YVAD-CMK (Cayman Chemical), which was at a final concentration of 100 µM/per 1 ml of whole blood, prior to dilution. Transfection was performed using X-treme GENE siRNA transfection reagent (Roche) for small interfering RNA (siRNA) against MIAT (siMIAT), miR-214-3p mimics (miR-214-3p) and anti-miR-214-3p oligonucleotide (AMO-214-3p) with corresponding negative controls (si-NC, NC, and AMO-NC). The above products were designed and synthesized by RIO-BIO (Guangzhou, China). The sequences are listed in Table 3.

RNA isolation and quantitative real-time -PCR (qRT-PCR)

TRIzol LS and TRIzol (Invitrogen, Carlsbad, CA, USA) were used to extract total RNA from human serum and mice heart tissue. Reverse transcription was done using a reverse transcription kit (Toyobo, Osaka, Japan). The cDNA was amplified and detected by ABI 7500 fast real-time PCR system (Applied Bio-systems, CA, USA) using SYBR Green I (Yoyobo, Osaka, Japan). Each amplification and detection was performed by using a CFX96 Real Time PCR Detection system (Bio-Rad Laboratories, Inc., CA, USA). PCR array was performed under the following conditions: 95°C For 10 minutes, then 38 cycles at 95°C for 15 secocds and at 50°C for 1 minute. GAPDH was used as an internal standard for MIAT and mRNAs. U6 was used as an internal standard for miR-214-3p. The primer sequences of mice samples are found in Table 4.

Western blotting

Total protein samples were extracted from mice or cells. The total protein was extracted with the protein extraction kit (KGP250; Nanjing KeyGen Biotech Co., Ltd., Jiangsu, China). The protein (10 µg per lane) was separated on 10% SDS-PAGE, followed by transferring to nitrocellulose membranes. The membranes were blocked for 2 hours at room temperature and then incubated overnight at 4°C with one of the following primary antibodies: rabbit polyclonal anti-CASP1 (A0964; ABclonal), rabbit polyclonal anti-IL-1β (A20529; ABclonal), rabbit polyclonal anti-gasdermin D (GSDMD, 96458; Cell Signaling Technology, MA, USA), and rabbit monoclonal anti-GAPDH (A19056; ABclonal). All antibodies were diluted by TBST (cat. no. T1086; Solarbio) to 1:1,000. After washing, the membranes were incubated for 2 hours with goat anti-rabbit IgG antibody (AP132; Sigma-Aldrich; MO, USA). Bands were captured by GelDox XR system (Bio-Rad Laboratories, Inc.), and protein intensity was measured using Image Lab™ software (version 2.0.1; Bio-Rad Laboratories, Inc.).

Measurement of $[Ca^{2+}]_i$ in cardiomyocytes

Washed cardiomyocytes were taken up in standard Tyrode solution (NaCl 12.6 mmol/L, KCl 0.54 mmol/L, HEPES 1 mmol/L, NaH_2PO_4 0.033 mmol/L, $MgCl_2.6H_2O$ 0.1 mmol/L, $CaCl_2$ 1.8 mmol/L, and glucose 10 mmol/L, pH = 7.4). Cells were loaded with 10 µM Fluo 4/AM (Invitrogen) and Pluronic F-127 (Invitrogen) for 30 min at 37°C. The cells were then washed twice and stored in 1 mL of calcium solution. Images were captured by confocal microscopy (LSM-700; ZEISS, Baden-Württemberg, Germany). During this process, cells were stimulated with 50 µL of KCl. The fluorescence intensity (FI) of the cells was measured. The relative changes of $[Ca^{2+}]_i$ was calculated as $\Delta F/F_0 = (F_{max}-F_0)/F_0$.

Whole-cell patch clamp method

The cells were placed onto a temperature-controlled (20–25°C) recording chamber and perfused continuously with an extracellular solution (NaCl 13.6 mmol/L, KCl 0.54 mmol/L, $MgCl_2 \cdot 6H_2O$ 0.1 mmol/L, HEPES 1 mmol/L, glucose 0.1 mmol/L, $CaCl_2$ 0.18 mmol/L, $NaH_2PO_4 \cdot 2H_2O$ 0.033 mmol/L with NaOH to pH 7.37). Kraft-Brune solution was configured by L-glutamic acid 70.0 mmol/L, taurine 15.0 mmol/L, EGTA 0.5 mmol/L, KH_2PO_4 10.0 mmol/L, KCl 30.0 mmol/L, $MgCl_2 \cdot 6H_2O$ 0.5 mmol/L, HEPES 10.0 mmol/L, glucose 10.0 mmol/L with KOH to pH 7.20. The cells from mice atrial muscle were obtained by heart tissue collection, collagen digestion, and cells isolation. Axopatch 700B microelectrode amplifier (Axon Instruments Inc., CA, USA) was used to record the action potentials. They were evoked by a stimulus current of resistance growth from 0.5 to 300 MΩ, with the holding clamp potential from -20 to -60 mV. Finally, the action potential was obtained after releasing the holding potential in cell mode. All above process ran at room temperature. For each sample, 10 different recordings were made. Cells which have unstable currents were excluded from the analysis.

QUANTIFICATION AND STATISTICAL ANALYSIS

The data were analyzed by using SPSS version 19.0 (IBM, Corp., NM, USA). All data are expressed as mean ± standard deviation. Student's t-tests were used to determine the significance of differences between two groups, and one-way ANOVA and Tukey's post hoc test were used to determine differences among multiple groups. P<0.05 was considered to indicate a statistically significant difference. N representing the sample number in one tested group, was set to statistically eliminate the individual differences. Graphs were prepared in GraphPad Prism 8.0.